This article has been accepted for publication in a future issue of this journal, but has not been fully edited. Content may change prior to final publication. Citation information: DOI 10.1109/TIA.2022.3177175, IEEE Transactions on Industry Applications

Increasing RES Hosting Capacity in Distribution Networks Through Closed-Loop Reconfiguration and Volt/VAr Control

Juan M. Home-Ortiz, Leonardo H. Macedo, *Member, IEEE*, Renzo Vargas, *Member, IEEE*, Rubén Romero, *Senior Member, IEEE*, José Roberto Sanches Mantovani, *Member, IEEE*, and João P. S. Catalão, *Fellow, IEEE*

***Abstract*—This paper presents a novel mixed-integer second-order cone programming model to increase the photovoltaic (PV) hosting capacity and optimize the operation of distribution networks. The problem considers voltage and reactive (Volt/VAr) control through the optimal operation of capacitors banks, substations' on-load tap changers, voltage regulators, and network reconfiguration with radial and closed-loop operation topologies. The proposed formulation considers voltage-dependent models for loads and capacitor banks. The objective function maximizes the PV hosting capacity of the network. Numerical experiments are carried out using the 33-node and the 85-node networks. Results demonstrate the effectiveness of the proposed formulation to increase the penetration of PV sources, especially when the closed-loop operation is allowed, together with network reconfiguration and Volt/VAr control.**

***Keywords*—Closed-loop topology, distribution networks reconfiguration, mixed-integer second-order cone programming, PV hosting capacity, Volt/VAr control.**

NOMENCLATURE

Indices and sets:

i, j	Indices for nodes
ij, ji	Indices for branches
k	Index for capacitor banks' (CBs) modules
s	Index for stochastic scenarios
Γ_B	Set of branches
Γ_{CB}	Set of nodes with capacitor banks
Γ_{DG}	Set of nodes with dispatchable distributed generators (DGs)
Γ_N	Set of nodes
Γ_{PV}	Set of candidate nodes to install PV generation
Γ_S	Set of stochastic scenarios
Γ_{SS}	Set of substation (SS) nodes
Γ_{TC}	Set of branches with voltage regulators (VRs)/SSs' on-load tap changers (OLTCs)

Parameters:

B_i^{CB}	Susceptance of a CB's module installed at node i
e_i^{DG}, e_i^{SS}	CO_2 emissions intensity for dispatchable DGs and SSs at node i
$\overline{I}_{ij}$	Current capacity of branch ij
M^V, M^Θ	Big-M parameters used to calculate the slack variables associated with the voltage magnitude drop equation on a branch/the voltage phase angle difference across a branch
N^{LP}	Maximum number of basic loops allowed to be formed in the network
$P_{i,s}^D$, $Q_{i,s}^D$	Active/reactive power load at nominal voltage at node i, scenario s
$\underline{PF}_i^{DG}$, $\overline{PF}_i^{DG}$	Power factor limits of the dispatchable DG at node i
$\underline{PF}_i^{PV}$, $\overline{PF}_i^{PV}$	Power factor limits of the PV unit at node i
R_{ij}, X_{ij}, Z_{ij}	Resistance, reactance, and impedance of branch ij
$\overline{S}_i^{DG}$	Apparent power capacity of the dispatchable DG at node i
$\overline{S}_i^{SS}$	Apparent power capacity of the SS at node i
$\overline{V}$, $\underline{V}$	Maximum/minimum voltage magnitude limits allowed at the nodes of the network
V^N	Nominal voltage of the network
$\overline{n}_i^{CB}$	Number of CB's modules installed at node i
$\hat{v}_{i,s}$	Estimate of the voltage magnitude at node i, scenario s
Δ_s^T	Duration of stochastic scenario s
$\overline{\Delta}_{ij}^{TC}$	Regulation of the VR/SS's OLTC of branch ij
$\gamma_{i,s}^Z$, $\gamma_{i,s}^I$, $\gamma_{i,s}^P$	Participation factors of constant impedance/current/power of the active power demand at node i, scenario s
$\lambda_{i,s}^{PV}$	Generation factor of a PV unit at node i, scenario s
$\mu_{i,s}^Z$, $\mu_{i,s}^I$, $\mu_{i,s}^P$	Participation factors of constant impedance/current/power of the reactive power demand at node i, scenario s
ϖ	Total CO_2 emissions from the network
ψ_i	Energy curtailment limit for the PV unit at node i

Continuous variables:

$I_{ij,s}^{SQ}$	Square of the current magnitude on branch ij, scenario s
$P_{ij,s}$, $Q_{ij,s}$	Active/reactive power flows through branch ij, scenario s
$P_{i,s}^C$	Power curtailment for the PV generation unit at node i, scenario s
$P_{i,s}^{DG}$, $Q_{i,s}^{DG}$	Active/reactive power injected by the DG at node i, scenario s
$P_{i,s}^{PV}$, $Q_{i,s}^{PV}$	Active/reactive power injected by the PV generator at node i, scenario s
$\overline{P}_i^{PV}$	Installed PV capacity at node i
$P_{i,s}^{SS}$, $Q_{i,s}^{SS}$	Active/reactive power injected by the SS at node i, scenario s
$Q_{i,k,s}^{CB}$	Reactive power injected by the CB's module k, at node i, scenario s
$\hat{Q}_{i,s}^{CB}$	Total reactive power injected by the CB at node i, scenario s
$V_{i,s}$	Voltage magnitude at node i, scenario s

This work was supported in part by the Coordination for the Improvement of Higher Education Personnel (CAPES) – Finance Code 001, the Brazilian National Council for Scientific and Technological Development (CNPq), grants 305852/2017-5 and 304726/2020-6, the São Paulo Research Foundation (FAPESP), under grants 2015/21972-6, 2018/20355-1, 2019/01841-5, and 2019/23755-3, and by ENEL under the grant PEE-00390-1062/2017 - P&D-00390-1083-2020_UFABC, ANEEL 001-2016; and in part by FEDER funds through COMPETE 2020 and by Portuguese funds through FCT, under POCI-01-0145-FEDER-029803 (02/SAICT/2017).

J. M. Home-Ortiz, L. H. Macedo, R. Romero, and J. R. S. Mantovani are with the Department of Electrical Engineering, São Paulo State University, Ilha Solteira, 15385-000, SP, Brazil (e-mail: juan.home@unesp.br; leohfmp@ieee.org; ruben.romero@ unesp.br; mant@dee.feis.unesp.br).

R. Vargas is with the Engineering, Modeling and Applied Social Sciences Center, Federal University of ABC–UFABC, Santo André, 09210-580, SP, Brazil (e-mail: renzo@ieee.org).

J.P.S. Catalão is with the Faculty of Engineering of the University of Porto and INESC TEC, Porto, 4200-465, Portugal (e-mail: catalao@ubi.pt).

This article has been accepted for publication in a future issue of this journal, but has not been fully edited. Content may change prior to final publication. Citation information: DOI 10.1109/TIA.2022.3177175, IEEE Transactions on Industry Applications

$V_{i,s}^{SQ}$	Square of the voltage magnitude at node i, scenario s
f_{ij}	Fictitious flow on branch ij
g_i	Fictitious generation at the SS node i
$\delta_{ij,s}^{TC}$	Auxiliary variable for the voltage difference across the VR/SS's OLTC on branch ij, scenario s
$\zeta_{ij,s}$, $\xi_{ij,s}$	Slack variables for the calculation of the voltage drop/phase angle difference across branch ij, scenario s
$\theta_{i,s}$	Voltage phase angle at node i, scenario s

Binary variables:

w_{ij}^{SW}	Operational state of branch ij
$y_{i,k,s}^{CB}$	Indicates if the CB module k is operating ($y_{i,k,s}^{CB} = 1$) or not ($y_{i,k,s}^{CB} = 0$) at node i, scenario s

I. Introduction

Increased concerns on environmental issues have incentivized the inclusion of renewable energy sources (RES) in electrical distribution networks [1]. Encouraged by governmental incentives [2], CO_2 emissions mitigation strategies [3], reduction of electricity bills [4], and a continuous decrease in equipment costs [5], the presence of RES in distribution networks has increased over the years.

However, the introduction of these technologies in electric grids brings new challenges for the operational planners due to RES generation characteristics. These characteristics include an intermittent behavior, which has an impact on the voltage and current constraints of the networks [6], [7].

These impacts could limit the amount of RES insertion in distribution networks and could only be mitigated through investments to reinforce the network. As such, operational planners look for alternatives to adequate and improve the operation of distribution networks in order to increase the hosting capacity, i.e., the amount of RES that can be accommodated on a distribution network.

In recent years, several studies have assessed the hosting capacity problem. In [8], the authors recognize that a high penetration of photovoltaic (PV) systems can potentially cause several operational issues in distribution networks. In this sense, a Monte Carlo-based hourly stochastic analysis framework is presented to identify the PV accommodation limit in distribution networks. In [9], a distributionally robust optimization-based data-driven technique is employed to determine the hosting capacity for active distribution networks considering the uncertain forecasting errors of PV generation outputs and load demands. In [10], a bilevel optimization dispatch method based on an iterative particle swarm optimization (PSO) algorithm is proposed for the PV hosting capacity. In [11], a constructive model for hosting capacity determination is presented. For this purpose, solutions are constructed sequentially according to realistic constraints. In [12], a streamlined methodology is proposed to determine the amount of PV capacity that can be accommodated on a distribution feeder before undesirable impacts occur. This approach finalizes assigning a minimum and maximum hosting capacity value to each feeder under analysis.

Network reconfiguration is one of the most common approaches to improve the operation of distribution networks. It consists of performing switching operations with the objective of changing the topology of the network for alleviating congestions and improving the voltage profile while maintaining a radial configuration for the network. Reference [13] evaluates the possibility of performing network reconfiguration for improving the hosting capacity of distribution networks while maintaining a radial configuration. In [14], the authors formulate a network reconfiguration problem to minimize voltage violations associated with increasing PV penetration in a radial distribution network.

In [15], a two-stage optimization framework is presented based on the hypothesis that by decreasing the Thévenin impedance at the point of connection, a larger PV capacity can be integrated. The first stage aims to design a new optimal configuration for a distribution network. In the second stage, the PV hosting capacity is determined for the network configuration obtained in the first stage. In [16], a multiperiod network reconfiguration is presented for increasing the hosting capacity of distribution networks under a minimum required number of switching operations. The proposed four-stage method includes: assessment stage, time-partitioning stage, optimization stage, and evaluation stage.

Closed-loop operation topology is an alternative for radial operation in distribution networks. The advantages of a closed-loop operation include a potential decrease of electric losses [17] and reliability improvements in the normal state [18]. Several utilities have adopted normally closed-loop topologies to serve their customers, including Taipower Company, Florida Power Company, Hong Kong Electric Company, and Singapore Power [18]. The upgrading of primary feeders from open-loop to normally closed-loop arrangements aims to guarantee a reliable and high-quality power supply since some customers cannot afford either a short-period interruption or a long-duration voltage dip. Reference [18] discusses the requirements and drawbacks of transitioning from radial to closed-loop configurations in distribution systems. These requirements include the evaluation of short-circuit currents, capacities, and voltage levels of the substations; the ratings, impedances, loadings, and load characteristics of the substation transformers; the size, length, loading, load distribution, and load characteristics of the feeders. In contingency scenarios, the response of the system after a permanent fault is enhanced by reconnecting more loads to primary feeders [19]. In [17], the reconfiguration problem considering the closed-loop operation for minimizing electric losses is formulated as a mixed-integer nonlinear programming (MINLP) problem. A very important aspect of this work is that the authors verify that not necessarily an all-closed-switches operation configuration is the topology with the lowest value of power losses. In [20], the possibility of considering a closed-loop operation topology of the network for improving the integration of RES in distribution networks is analyzed, considering only the possibility of closing tie switches, i.e., without considering network reconfiguration.

Voltage and reactive (Volt/VAr) control is another option to improve the operation of distribution networks. It consists of determining the optimal adjustment of the tap positions of the substations' (SSs) on-load tap changers (OLTCs), voltage regulators (VRs), and the determination of the number of capacitor banks (CBs) in operation at each node. Reference [21] proposes a mathematical formulation to improve the hosting capacity of active distribution networks through Volt/VAr control without changing the network topology.

In [22], the maximum hosting capacity of a network is evaluated using a robust optimization-based method considering the operation of OLTCs and static var compensators. In

[23], an optimization-based framework is proposed to assess the impact of active distribution network management schemes in increasing the PV hosting capacity, including PV-based and OLTC-based control strategies. In [24], a mathematical model is proposed to maximize the distribution network hosting capacity by using OLTC control and grid reconfiguration to manage grid operation conditions related to voltage rise problems. In [25], a genetic algorithm-based technique is developed to maximize the PV hosting capacity of 17 utility distribution feeders by optimally switching CBs, adjusting VRs taps, managing controllable branch switches, and controlling smart PV inverters.

In this work, we consider network reconfiguration, Volt/VAr control, and closed-loop operation for increasing the maximum penetration of RES in distribution networks. Different from [20], the proposed approach considers opening sectionalizing switches to provide more flexibility to the network operation. The proposed formulation consists of a new mixed-integer second-order cone programming (MISOCP) model. To handle the uncertainties of RES, a stochastic scenario-based formulation is used. The load is represented using the voltage-dependent ZIP model to characterize a more realistic representation of the problem. The objective function considers the maximization of the penetration of RES in the distribution networks in order to mitigate CO_2 emissions.

This paper significantly extends [1] by including an expanded literature review, a much more detailed explanation of the proposed mathematical model, and presenting comprehensive results using the 85-node distribution network.

Hence, the main contributions of this work are as follows:

- From a modeling perspective, a new stochastic-programming-based model is proposed to determine the optimal distribution network topology, allowing closed-loop operation and Volt/VAr control, in order to increase the PV hosting capacity of the network and reduce the associated CO_2 emissions;
- From a methodological perspective, the resulting MINLP problem is recast in order to obtain a relaxed MISOCP model that is treatable, scalable, and can be effectively solved by commercial solvers.

The remainder of the paper is organized as follows: Section II presents the proposed formulation for the problem; the results of the tests conducted using the 33-node network and the 85-node network are presented in Section III; finally, the conclusions of the work are presented in Section IV.

II. MISOCP Model for the Problem

The formulation that maximizes the PV hosting capacity of the network is presented in this section.

A. Objective Function

The objective function $\mathcal{F}$ is presented in (1).

$$\text{maximize}\, \mathcal{F} = \sum_{i \in \Gamma_{PV}} \overline{P}_i^{PV} \tag{1}$$

Equation (1) maximizes the total PV generation installed capacity in the network, accounting for all candidate nodes to install PV units.

B. Power Flow Constraints

The ac operation of the network is represented by the power flow constraints (2)–(9) which consider a voltage-dependent formulation for the load [19].

$$\sum_{ji \in \Gamma_B} P_{ji,s} - \sum_{ij \in \Gamma_B} \left(P_{ij,s} + R_{ij} I_{ij,s}^{SQ}\right) + P_{i,s}^{SS} + P_{i,s}^{DG} + P_{i,s}^{PV} = P_{i,s}^{D} \left[\gamma_{i,s}^{Z} \frac{V_{i,s}^{SQ}}{(V^N)^2} + \gamma_{i,s}^{I} \frac{V_{i,s}}{V^N} + \gamma_{i,s}^{P}\right] \tag{2}$$

$$\sum_{ji \in \Gamma_B} Q_{ji,s} - \sum_{ij \in \Gamma_B} \left(Q_{ij,s} + X_{ij} I_{ij,s}^{SQ}\right) + Q_{i,s}^{SS} + Q_{i,s}^{DG} + Q_{i,s}^{PV} + \hat{Q}_{i,s}^{CB} = Q_{i,s}^{D} \left[\mu_{i,s}^{Z} \frac{V_{i,s}^{SQ}}{(V^N)^2} + \mu_{i,s}^{I} \frac{V_{i,s}}{V^N} + \mu_{i,s}^{P}\right] \tag{3}$$

$$V_{i,s} = \sqrt{\frac{\overline{V} + \underline{V}}{2}} + \frac{1}{2\sqrt{\frac{\overline{V} + \underline{V}}{2}}} \left(V_{i,s}^{SQ} - \frac{\overline{V} + \underline{V}}{2}\right) \tag{4}$$

$$\forall i \in \Gamma_N, s \in \Gamma_S$$

$$V_{i,s}^{SQ} - V_{j,s}^{SQ} + \delta_{ij,s}^{TC} + \zeta_{ij,s} = 2(R_{ij} P_{ij,s} + X_{ij} Q_{ij,s}) + Z_{ij}^2 I_{ij,s}^{SQ} \tag{5}$$

$$\hat{\upsilon}_{i,s} \hat{\upsilon}_{j,s} (\theta_{i,s} - \theta_{j,s} + \xi_{ij,s}) = X_{ij} P_{ij,s} - R_{ij} Q_{ij,s} \tag{6}$$

$$V_{j,s}^{SQ} I_{ij,s}^{SQ} \geq P_{ij,s}^2 + Q_{ij,s}^2 \tag{7}$$

$$|\zeta_{ij,s}| \leq M^V (1 - w_{ij}^{SW}) \tag{8}$$

$$|\xi_{ij,s}| \leq M^\Theta (1 - w_{ij}^{SW}) \tag{9}$$

$$\forall ij \in \Gamma_B, s \in \Gamma_S$$

Constraints (2) and (3) are, respectively, the active and reactive power balance constraints, representing the application of Kirchhoff's current law to the network. The voltage-dependent ZIP model [26] is used in this formulation to represent the load. Constraint (4) calculates the voltage magnitude at node i, scenario s, from the value of the squared voltage magnitude, $V_{i,s}^{SQ}$, using a Taylor's series expansion of the square root of $V_{i,s}^{SQ}$ at the midpoint of the voltage magnitude limits $(\overline{V} + \underline{V})/2$.

Constraints (5)–(9) represent the systematic application of Kirchhoff's voltage law to the network. Constraint (5) calculates the difference of the values of the squared voltage magnitudes $V_{i,s}^{SQ}$ and $V_{j,s}^{SQ}$ across branch ij in scenario s, as a function of the active and reactive power flows, the squared value of the current magnitude, and the parameters of the line. The variable $\delta_{ij,s}^{TC}$ is related to the operation of the SS's OLTCs and VRs and will be described later. The slack variable $\zeta_{ij,s}$ is used to ignore the calculation of the difference of the values of the squared voltage magnitudes across branch ij when the switch associated with branch ij is open.

Constraint (6) calculates the voltage phase angle difference, $\theta_{i,s} - \theta_{j,s}$, across branch ij in scenario s, as a function of the active and reactive power flows on the branch and the parameters of the line. This constraint is a linearization of the original nonlinear one $\sqrt{V_{i,s} V_{j,s}} \sin(\theta_{i,s} - \theta_{j,s} + \xi_{ij,s}) = X_{ij} P_{ij,s} - R_{ij} Q_{ij,s}$. Similar to $\zeta_{ij,s}$ in (5), the slack variable $\xi_{ij,s}$ is used to ignore the calculation of the voltage phase angle when the switch associated with branch ij is open, i.e., the

This article has been accepted for publication in a future issue of this journal, but has not been fully edited. Content may change prior to final publication. Citation information: DOI 10.1109/TIA.2022.3177175, IEEE Transactions on Industry Applications

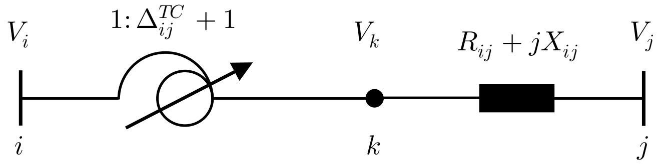

Fig. 1 Equivalent circuit of a VR/SS's OLTC.

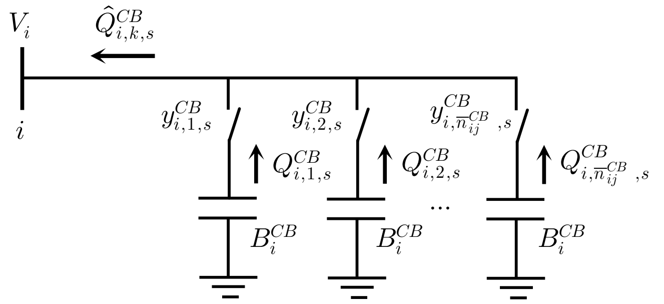

Fig. 2 Illustration of the operation of a CB.

voltage phase angles at buses i and j in scenario s are not directly related to the power flow and parameters of branch ij if the switch of branch ij is open.

Constraint (7) is a second-order cone constraint that calculates the squared value of the current magnitude on branch ij, scenario s, as a function of the squared values of the active and reactive power flows on the branch and the squared value of the voltage magnitude at the terminal node j of the branch in scenario s. Ideally, this constraint should be active in the solution, otherwise, the terms $R_{ij}I_{ij,s}^{SQ}$, $X_{ij}I_{ij,s}^{SQ}$, and $Z_{ij}^2 I_{ij,s}^{SQ}$ in (2), (3), and (5) will be overestimated, leading to higher values of losses. Note, however, that the impact of (7) not being active in the solution is limited, since the losses are only a small fraction of the total load in a distribution system. In this paper, the feasibility of the solution is evaluated using a power flow algorithm.

Constraints (8) and (9) are used to calculate the slack variables $\zeta_{ij,}$ and $\xi_{ij,s}$ according to the statuses of the switches. Note that if $w_{ij}^{SW}=0$, indicating an open switch status, then $-M^V \le \zeta_{ij,s} \le M^V$ and $-M^\Theta \le \xi_{ij,s} \le M^\Theta$, and in (5) and (6) the voltage magnitudes and voltage phase angles calculation at the terminal nodes i and j will not depend on the power flow on branch ij. On the other hand, if $w_{ij}^{SW}=1$, indicating a closed switch status, then $\zeta_{ij,s}=0$ and $\xi_{ij,}\ =0$, and (5) and (6) will calculate the values of the voltage magnitudes and voltage phase angles at the terminal nodes i and j according to values of the power flow (and current magnitude) on branch ij.

C. Physical and Operational Limits of the Network

Constraints (10)–(14) are the physical and operational limits of the network.

$$0 \le I_{ij,s}^{SQ} \le \overline{I}_{ij}^2 w_{ij}^{SW} \qquad \forall ij \in \Gamma_B, s \in \Gamma_S \qquad (10)$$

$$|P_{ij,s}| \le \overline{VI}_{ij} w_{ij}^{SW} \qquad \forall ij \in \Gamma_B, s \in \Gamma_S \qquad (11)$$

$$|Q_{ij,s}| \le \overline{VI}_{ij} w_{ij}^{SW} \qquad \forall ij \in \Gamma_B, s \in \Gamma_S \qquad (12)$$

$$\underline{V}^2 \le V_{i,s}^{SQ} \le \overline{V}^2 \qquad \forall i \in \Gamma_N, s \in \Gamma_S \qquad (13)$$

$$(P_{i,s}^{SS})^2 + (Q_{i,s}^{SS})^2 \le \left(\overline{S}_i^{SS}\right)^2 \qquad \forall i \in \Gamma_{SS}, s \in \Gamma_S \qquad (14)$$

According to the switches statuses, constraints (10)–(12) define the current capacities, active, and reactive limits for the branches, (13) is the voltage limit for the nodes, and (14) is the apparent power capacity of the SSs.

Note that in (10)–(12), if $w_{ij}^{SW}=0$, then the values of $I_{ij,s}^{SQ}$, $P_{ij,s}$, and $Q_{ij,s}$ will also be zero. On the other hand, if $w_{ij}^{SW}=1$, then $I_{ij,s}^{SQ}$, $P_{ij,s}$, and $Q_{ij,s}$ can assume any values within their bounds (related to the current capacity of the lines). Moreover, (10) together with (7) are sufficient to ensure that $P_{ij,s}=0$ and $Q_{ij,s}=0$ if $w_{ij}^{SW}=0$. However, (11) and (12) are included in the model because they improve the convergence speed of the optimization solver.

Since $V_{i,s}^{SQ}$ is directly available in the formulation, (13) considers the squared values of $\underline{V}$ and $\overline{V}$ to limit $V_{i,s}^{SQ}$.

D. Operation of the SSs' OLTCs and VRs

The operation of SSs' OLTCs and VRs can be modeled considering discrete tap steps. However, a discrete representation increases the complexity of the problem. Therefore, a continuous formulation of the tap of SSs' OLTCs and VRs is considered in this paper.

Consider an ideal transformer with a tap ratio $1{:}\,\Delta_{ij}^{TC}+1$ in series with the transformer impedance $R_{ij}+jX_{ij}$, presented in Fig. 1.

The calculation of the square of the voltage magnitude at node k is shown in (15), while (16) defines δ_{ij}^{TC}, the difference between the squared value of the voltage magnitudes at nodes k and i.

$$V_k^2 = (\Delta_{ij}^{TC}+1)^2 V_i^2 \qquad (15)$$

$$\delta_{ij}^{TC} = V_k^2 - V_i^2 = \Delta_{ij}^{TC}(\Delta_{ij}^{TC}+2)V_i^2 \qquad (16)$$

Equation (17) shows how to obtain the value of the tap from δ_{ij}^{TC} and V_i.

$$\Delta_{ij}^{TC}+1 = \frac{\sqrt{V_i^2+\delta_{ij}^{TC}}}{V_i} \qquad (17)$$

Based on these considerations, the operation of the SSs' OLTCs and VRs is modeled in (18) [19].

$$|\delta_{ij,s}^{TC}| \le \overline{\Delta}_{ij}^{TC}(\overline{\Delta}_{ij}^{TC}+2)V_{i,s}^{SQ} \qquad \forall ij \in \Gamma_{TC}, s \in \Gamma_S \qquad (18)$$

Constraint (18) calculates $\delta_{ij,s}^{TC}$ considering the voltage $V_{i,s}^{SQ}$ and $\overline{\Delta}_{ij}^{TC}$.

The error associated with the consideration of continuous taps will depend on the number of tap positions of the VR.

Consider a typical VR with 33 tap positions (±16 positions and a position 0) and a maximum regulation $\overline{\Delta}_{ij}^{TC}=0.1$. The maximum error that will be verified in this situation will be when the continuous tap remains exactly between two discrete positions, and the value of the maximum error will be $0.1/(2\times 33)=0.15\%$.

E. Operation of CBs

The operation of the CBs is formulated using a voltage-dependent model, as presented in (19)–(21). Fig. 2 illustrates the operation of a CB installed at node i.

$$\hat{Q}_{i,s}^{CB} = \sum_{k=1}^{\overline{n}_i^{CB}} Q_{i,k,s}^{CB} \qquad \forall i \in \Gamma_{CB}, s \in \Gamma_S \qquad (19)$$

This article has been accepted for publication in a future issue of this journal, but has not been fully edited. Content may change prior to final publication. Citation information: DOI 10.1109/TIA.2022.3177175, IEEE Transactions on Industry Applications

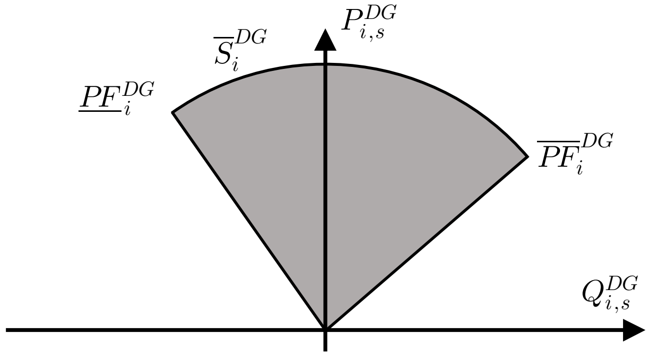

Fig. 3 Capability curve of a dispatchable DG.

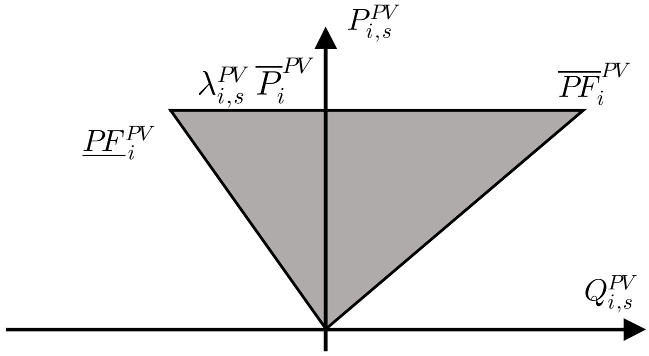

Fig. 4 Capacity of a PV unit.

$$-B_i^{CB}\overline{V}^2(1-y_{i,k,s}^{CB}) \le Q_{i,k,s}^{CB} - B_i^{CB}V_{i,s}^{SQ} \le -B_i^{CB}\underline{V}^2(1-y_{i,k,s}^{CB}) \quad (20)$$

$$B_i^{CB}\underline{V}^2 y_{i,k,s}^{CB} \le Q_{i,k,s}^{CB} \le B_i^{CB}\overline{V}^2 y_{i,k,s}^{CB} \quad (21)$$

$$\forall i \in \Gamma_{CB}, k \in \{1, \cdots, \overline{n}_{ij}^{CB}\}, s \in \Gamma_S$$

Constraint (19) calculates the total reactive power injected by a CB at node i, scenario s, as the sum of the reactive power injected by each module k.

The disjunctive constraints (20) and (21) calculate the reactive power injected by each CB module k. Note that, if $y_{i,k,s}^{CB} = 0$, then $Q_{i,k,s}^{CB} = 0$ in (21) and $V_{i,s}^{SQ}$ is limited to its bounds in (20). On the other hand, if $y_{i,k,s}^{CB} = 1$, then $Q_{i,k,s}^{CB} = B_i^{CB}V_{i,s}^{SQ}$ in (20) while (21) provides the limits for $Q_{i,k,s}^{CB}$, that will be always satisfied.

F. Dispatchable distributed generators (DGs)

The capacities of the dispatchable DGs are considered in (22)–(24).

Fig. 3 illustrates the capability curve of a dispatchable DG, modeled as a synchronous machine.

$$(P_{i,s}^{DG})^2 + (Q_{i,s}^{DG})^2 \le \left(\overline{S}_i^{DG}\right)^2 \qquad \forall i \in \Gamma_{DG}, s \in \Gamma_S \quad (22)$$

$$P_{i,s}^{DG} \ge 0 \qquad \forall i \in \Gamma_{DG}, s \in \Gamma_S \quad (23)$$

$$-P_{i,s}^{DG}\tan(\cos^{-1}(\underline{PF}_i^{DG})) \le Q_{i,s}^{DG} \le P_{i,s}^{DG}\tan(\cos^{-1}(\overline{PF}_i^{DG})) \quad (24)$$

$$\forall i \in \Gamma_{DG}, s \in \Gamma_S$$

The quadratic constraint (22) is the apparent power generation capacity of the DGs, (23) requires that a DG can only inject active power into the network, and (24) is the power factor limit for the DGs.

G. Topological Constraints

The network connectivity and the maximum number of basic loops allowed to be formed are controlled by (25)–(28) through fictitious demands that must be attended at all nodes.

$$|\Gamma_N| - |\Gamma_{SS}| \le \sum_{ij \in \Gamma_B} w_{ij}^{SW} \le |\Gamma_N| - |\Gamma_{SS}| + N^{LP} \quad (25)$$

$$\sum_{ji \in \Gamma_B} f_{ji} - \sum_{ij \in \Gamma_B} f_{ij} + g_i = 1 \qquad \forall i \in \Gamma_N \quad (26)$$

$$|f_{ij}| \le (|\Gamma_N| - |\Gamma_{SS}|)w_{ij}^{SW} \qquad \forall ij \in \Gamma_B \quad (27)$$

$$0 \le g_i \le |\Gamma_N| \qquad \forall i \in \Gamma_{SS} \quad (28)$$

Constraint (25) controls the maximum number of basic loops in the network together with (26)–(28), that ensure the connectivity of the network, i.e., that there must be a path from each node of the network to an SS. Note that the model defines a single topology for the network that is adequate to operate in all scenarios.

Since the network is connected [ensured by (26)–(28)], constraint (25) is used to control the maximum number of basic loops in the network. The sum in (25) is equal to the number of branches with a closed switch. On the left-hand side of this constraint, we have $|\Gamma_N| - |\Gamma_{SS}|$, i.e., the cardinality of the set of nodes minus the cardinality of the set of SS nodes, which is equal to the number of load nodes. According to [27], $|\Gamma_N| - |\Gamma_{SS}|$ is the number of switches that must be closed so that a connected topology is radial. On the right-hand side of (25) we have $|\Gamma_N| - |\Gamma_{SS}| + N^{LP}$, where N^{LP} is the number of basic loops allowed to be formed in the network. Therefore, by letting $N^{LP} = 0$ we will obtain a radial topology for the network and by increasing N^{LP} we can obtain topologies with at most N^{LP} basic loops. This constraint is, therefore, used to control the topology of the network, together with (26)–(28), so that we do not obtain topologies with islanded nodes connected to DGs.

Constraint (26) is a balance equation for the fictitious flows, which requires that the total value of fictitious flows entering a node is equal to the total value of fictitious flows leaving a node. This equation is, therefore, the application of Kirchhoff's current law to the fictitious flows.

Constraint (27) limits the fictitious flow on branch ij according to its status: if $w_{ij}^{SW} = 0$, then $f_{ij} = 0$, else, if $w_{ij}^{SW} = 1$, $-(|\Gamma_N| - |\Gamma_{SS}|) \le f_{ij} \le (|\Gamma_N| - |\Gamma_{SS}|)$. Note that, since each node has a unity fictitious demand, the maximum fictitious flow through a branch is going to be equal to the number of load nodes.

Constraint (28) limits the fictitious generations at the SS nodes, g_i, to the number of nodes in the network. Since each node has a fictitious unity demand, the SSs must be able to satisfy this demand. The total fictitious demand in the network is, therefore, equal to the cardinality of the set of nodes, $|\Gamma_N|$, used as an upper bound for g_i. For the load nodes ($\{\Gamma_N - \Gamma_{SS}\}$), $g_i = 0$.

H. PV Hosting Capacity

The PV hosting capacity model is described in (29)–(32), while (33) calculates the total emissions from the network. Fig. 4 illustrates the capacity curve of a PV unit.

$$P_{i,s}^{PV} = \lambda_{i,s}^{PV}\overline{P}_i^{PV} - P_{i,s}^{C} \qquad \forall i \in \Gamma_{PV}, s \in \Gamma_S \quad (29)$$

This article has been accepted for publication in a future issue of this journal, but has not been fully edited. Content may change prior to final publication. Citation information: DOI 10.1109/TIA.2022.3177175, IEEE Transactions on Industry Applications

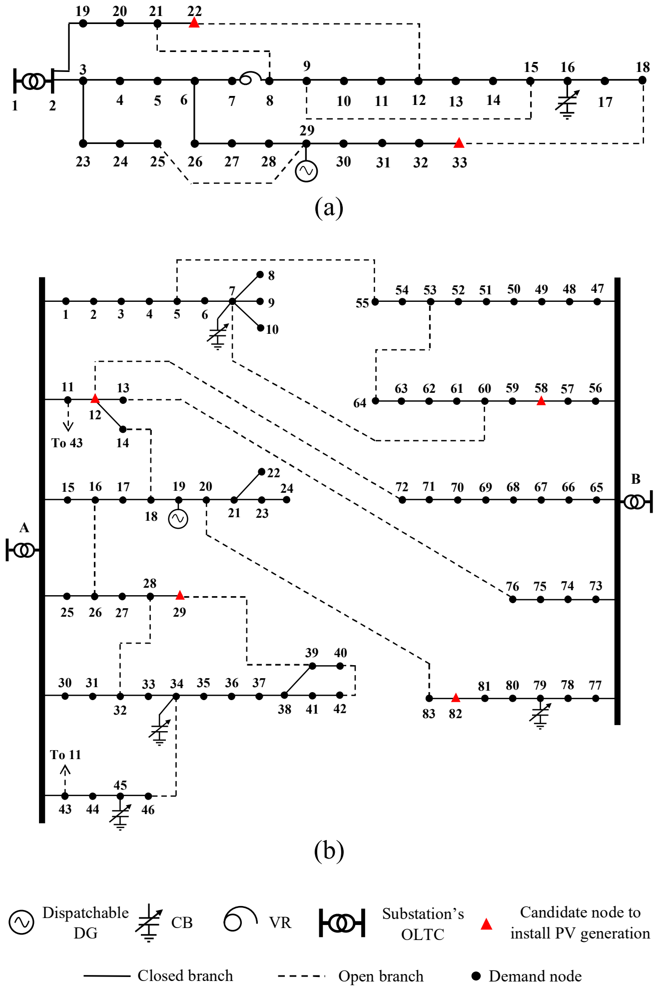

Fig. 5 Initial configuration of the (a) 33-node and (b) 85-node networks.

$$0 \le P^{C}_{i,s} \le \lambda^{PV}_{i,s}\overline{P}^{PV}_{i} \qquad \forall i \in \Gamma_{PV}, s \in \Gamma_S \tag{30}$$

$$-P^{PV}_{i,s}\tan(\cos^{-1}(\underline{PF}^{PV}_{i})) \le Q^{PV}_{i,s} \le P^{PV}_{i,s}\tan(\cos^{-1}(\overline{PF}^{PV}_{i})) \tag{31}$$

$$\forall i \in \Gamma_{PV}, s \in \Gamma_S$$

$$\sum_{s\in\Gamma_S}\Delta^{T}_{s}P^{C}_{i,s} \le \psi_i \sum_{s\in\Gamma_S}\Delta^{T}_{s}\lambda^{PV}_{i,s}\overline{P}^{PV}_{i} \qquad \forall i \in \Gamma_{PV} \tag{32}$$

$$\varpi = \sum_{i\in\Gamma_N}\sum_{s\in\Gamma_S}\Delta^{T}_{s}(e^{SS}_{i}P^{SS}_{i,s} + e^{DG}_{i}P^{DG}_{i,s}) \tag{33}$$

Constraint (29) determines the active power injected by the PV unit at node i according to the availability of the renewable resource in scenario s, given by the parameter $0 \le \lambda^{PV}_{i,s} \le 1$, the installed capacity $\overline{P}^{PV}_{i}$, and the active power curtailment $P^{C}_{i,s}$.

The power curtailment is constrained in (30), again according to the maximum generation capacity of the PV unit and the availability of the renewable resource in scenario s. The reactive power injected by the PV unit is limited in (31).

The total energy curtailment is limited according to (32). Note that the left-hand side of (32) provides the total energy curtailment for a period, while the right-hand side of this constraint is equal to the curtailment limit, $0 \le \psi_i \le 1$, multiplied by the total value of the available energy (which is a function of the PV installed capacity). Therefore, when $\psi_i = 0$, no PV generation curtailment is allowed, and when $\psi_i = 1$ the model allows any value of curtailment (up to the maximum capacity available).

Finally, the total CO_2 emissions from the network is calculated in (33).

In the proposed formulation, the objective function (1) is linear, as well as constraints (2)–(6), (8)–(13), (18)–(21), and (23)–(33). Constraint (7) is a second-order cone constraint, while (14) and (22) are quadratic constraints. Due to the presence of the binary variables w^{SW}_{ij} and $y^{CB}_{i,k,s}$, the resulting formulation is an MISOCP model, which can be solved by off-the-shelf optimization solvers.

III. Tests and Results

The proposed model is tested using a modified version of the 33-node network [28] shown in Fig. 5 (a), which operates at 12.66 kV and has a peak load of 6,092.62 kVA. This network has a 250 kVA dispatchable DG at node 29 with $\underline{PF}^{DG}_{i} = \overline{PF}^{DG}_{i} = 0.8$. A switchable CB with two 150 kVAr modules is installed at node 16. A VR is installed at branch 7–8, with a maximum regulation of 10% and ±16 positions, while the OLTC at the SS has ±16 positions with a maximum regulation of 5%. Nodes 22 and 33 are candidates for the installation of PV generation, for which $\underline{PF}^{PV}_{i} = 0.95$ and $\overline{PF}^{PV}_{i} = 0.90$, and the maximum curtailment allowed is $\psi_i =$ 10%.

Moreover, the proposed model is also tested on a modified version of the 85-node network [29], presented in Fig. 5 (b). This network has two SSs operating at 11.4 kV, one 250 kVA dispatchable DG at node 19 with $\underline{PF}^{DG}_{i} = \overline{PF}^{DG}_{i} = 0.8$, four CBs at nodes 7, 34, 45, and 79, each of them with two 300 kVAr modules, and a peak load of 45,451.21 kVA. Nodes 12, 29, 58, and 82 were selected to install PV generation, considering power factor limits of $\underline{PF}^{PV}_{i} = 0.95$ and $\overline{PF}^{PV}_{i} = 0.90$, and a maximum curtailment allowed of $\psi_i = 10\%$.

For both networks, the SS emissions factor is $e^{SS}_{i} = 2.17$ kg CO_2/kWh, the DG emissions factor is $e^{DG}_{i} = 0.63$ kg CO_2/kWh and the maximum and minimum voltage limits are 1.05 p.u. and 0.95 p.u., respectively. To represent the load behavior and solar irradiation, historical data of a year are obtained from [30] and the *k*-means clustering technique is used to reduce it to a suitable set of 24 scenarios using the procedure described in [3].

The proposed formulation was implemented in AMPL [31] and solved with the commercial solver CPLEX v20.1.0 [32] on a computer with a 3.2 GHz Intel® Core™ i7–8700 processor and 32 GB of RAM. Complete data for both networks are available in [33].

A. Study Cases

The maximization of the PV hosting capacity of the network is analyzed considering the following four cases:

I. Without considering network reconfiguration (the closed switches of the initial configuration of the network cannot be opened) and without considering Volt/VAr control (the adjustments of the SS's OLTC, VR, and CB are fixed at their initial states)—as proposed in [20];

II. Without considering network reconfiguration and considering Volt/VAr control (optimizing the operation of the SS's OLTC, VR, and CB)—this proposal is presented in [21] only for radial configurations;

This article has been accepted for publication in a future issue of this journal, but has not been fully edited. Content may change prior to final publication. Citation information: DOI 10.1109/TIA.2022.3177175, IEEE Transactions on Industry Applications

TABLE I
RESULTS FOR THE 33-NODE NETWORK – CASE I: WITHOUT CONSIDERING NETWORK RECONFIGURATION AND VOLT/VAR CONTROL

Results	Radial	1 Loop	2 Loops	3 Loops	4 Loops	5 Loops
Total PV generation installed (kW)	5,947.36	10,033.56	10,243.76	10,366.62	10,470.46	10,504.21
PV generation installed at nodes 22/33 (kW)	1,815.42/4,131.94	5,948.31/4,085.25	3,833.30/6,410.45	3,974.40/6,392.21	3,484.96/6,985.50	4,479.78/6,024.43
Open switches	8-21, 9-15, 12-22, 18-33, 25-29	8-21, 9-15, 18-33, 25-29	8-21, 9-15, 25-29	9-15, 25-29	25-29	–
Emissions from the main grid (tonnes)	59,260.18	47,353.86	46,907.22	47,029.09	46,975.92	46,886.86
Emissions from the DG (tonnes)	1,016.79	793.18	853.53	796.39	792.82	796.27
Total emissions (tonnes)	60,276.98	48,147.04	47,760.75	47,825.48	47,768.74	47,683.13

TABLE II
RESULTS FOR THE 33-NODE NETWORK – CASE II: WITHOUT CONSIDERING NETWORK RECONFIGURATION AND CONSIDERING VOLT/VAR CONTROL

Results	Radial	1 Loop	2 Loops	3 Loops	4 Loops	5 Loops
Total PV generation installed (kW)	8,254.36	10,174.00	10,318.03	10,422.54	10,491.57	10,530.28
PV generation installed at nodes 22/33 (kW)	4,209.21/4,045.15	6,087.87/4,086.13	6,345.10/3,972.94	6,449.42/3,973.12	3,594.85/6,896.72	3,942.03/6,588.25
Open switches	8-21, 9-15, 12-22, 18-33, 25-29	8-21, 9-15, 18-33, 25-29	9-15, 18-33, 25-29	18-33, 25-29	25-29	–
Emissions from the main grid (tonnes)	45,580.13	46,452.71	45,607.38	45,484.46	45,426.47	41,181.94
Emissions from the DG (tonnes)	1,193.61	614.61	804.69	797.51	788.06	840.54
Total emissions (tonnes)	46,773.74	47,067.32	46,412.07	46,281.97	46,214.53	42,022.48

TABLE III
RESULTS FOR THE 33-NODE NETWORK – CASE III: CONSIDERING NETWORK RECONFIGURATION AND NOT CONSIDERING VOLT/VAR CONTROL

Results	Radial	1 Loop	2 Loops	3 Loops	4 Loops	5 Loops
Total PV generation installed (kW)	10,224.64	10,396.16	10,426.75	10,457.46	10,490.64	10,504.21
PV generation installed at nodes 22/33 (kW)	5,536.47/4,688.17	4,087.32/6,308.83	3,829.94/6,596.81	3,516.82/6,940.63	4,529.65/5,961.00	4,479.78/6,024.43
Open switches	6-7, 14-15, 15-16, 8-21, 25-29	6-7, 10-11, 14-15, 25-29	10-11, 14-15, 25-29	10-11, 25-29	10-11	–
Emissions from the main grid (tonnes)	46,855.22	46,852.33	46,958.45	46,932.86	46,892.29	46,886.86
Emissions from the DG (tonnes)	807.86	823.60	807.85	809.06	799.56	796.27
Total emissions (tonnes)	47,663.07	47,675.93	47,766.30	47741.92	47,691.85	47,683.13

TABLE IV
RESULTS FOR THE 33-NODE NETWORK – CASE IV: CONSIDERING BOTH NETWORK RECONFIGURATION AND VOLT/VAR CONTROL

Results	Radial	1 Loop	2 Loops	3 Loops	4 Loops	5 Loops
Total PV generation installed (kW)	10,262.46	10,428.75	10,437.92	10,484.10	10,512.72	10,530.28
PV generation installed at nodes 22/33 (kW)	5,550.09/4,712.37	4,181.86/6,246.90	3,738.27/6,699.65	3,974.24/6,509.86	3,924.21/6,588.51	3,942.03/6,588.25
Open switches	6-7, 8-9, 10-11, 15-16, 25-29	6-7, 10-11, 14-15, 25-29	10-11, 14-15, 28-29	10-11, 14-15	10-11	–
Emissions from the main grid (tonnes)	42,464.53	42,007.52	41,608.38	41,312.00	41,373.60	41,181.94
Emissions from the DG (tonnes)	807.65	793.46	829.96	819.45	794.51	840.54
Total emissions (tonnes)	43,272.19	42,800.98	42,438.33	42,131.45	42,168.12	42,022.48

III. Considering network reconfiguration and without considering Volt/VAr control;

IV. Considering both network reconfiguration and Volt/VAr control—as proposed in this paper.

In all cases, it is considered the closed-loop operation of the network.

B. Discussion of the Results

1) 33-node network

Tables I–IV present the total hosting capacities for PV generation in the 33-node network obtained for Cases I–IV, respectively. These tables also provide the maximum capacities for PV generation integration at nodes 22 and 33, the configurations of the network, represented by the open switches, and information on the expected values of CO_2 emissions for each case.

By analyzing Table I, it can be verified that the maximum value of PV generation that can be integrated into the 33-node network is 5,947.36 kW considering the initial topology of the network without performing Volt/VAr control. It can also be verified that the maximum penetration of PV generation can be increased by a further 68.71%, to 10,033.56 kW, by only closing branch 12-22, therefore forming one loop in the

This article has been accepted for publication in a future issue of this journal, but has not been fully edited. Content may change prior to final publication. Citation information: DOI 10.1109/TIA.2022.3177175, IEEE Transactions on Industry Applications

TABLE V
RESULTS FOR THE 85-NODE NETWORK – CASE I: WITHOUT CONSIDERING NETWORK RECONFIGURATION AND VOLT/VAR CONTROL

Results	Radial	1 Loop	12 Loops
Total PV generation installed (kW)	53,578.06	61,061.49	65,461.19
PV generation installed at nodes 12/29/58/82 (kW)	16,754.44/ 11,123.91/ 14,006.59/ 11,693.12	24,238.44/ 11,123.33/ 14,006.59/ 11,693.12	29,544.68/ 8,181.54/ 10,445.84/ 17,289.14
Open switches	5-55, 7-60, 11-43, 12-72, 13-76, 14-18, 16-26, 20-83, 28-32, 29-39, 34-46, 40-42, 53-64	5-55, 7-60, 11-43, 12-72, 13-76, 16-26, 20-83, 28-32, 29-39, 34-46, 40-42, 53-64	34-46
Emissions from the main grid (tonnes)	377,574.69	351,003.46	343,590.55
Emissions from the DG (tonnes)	682.99	565.61	712.05
Total emissions (tonnes)	378,257.68	351,569.06	344,302.60

TABLE VI
RESULTS FOR THE 85-NODE NETWORK – CASE II: WITHOUT CONSIDERING NETWORK RECONFIGURATION AND CONSIDERING VOLT/VAR CONTROL

Results	Radial	1 Loop	12 Loops
Total PV generation installed (kW)	53,703.35	62,466.25	66,590.01
PV generation installed at nodes 12/29/58/82 (kW)	16,758.07/ 11,120.58/ 13,986.65/ 11,838.05	16,514.86/ 10,957.57/ 13,743.88/ 21,249.94	25,078.38/ 10,968.50/ 11,252.74/ 19,290.38
Open switches	5-55, 7-60, 11-43, 12-72, 13-76, 14-18, 16-26, 20-83, 28-32, 29-39, 34-46, 40-42, 53-64	5-55, 7-60, 11-43, 12-72, 13-76, 14-18, 16-26, 28-32, 29-39, 34-46, 40-42, 53-64	53-64
Emissions from the main grid (tonnes)	375,974.38	348,413.09	339,894.52
Emissions from the DG (tonnes)	953.53	669.59	653.41
Total emissions (tonnes)	376,927.91	349,082.68	340,547.93

network. Moreover, by closing more branches, the maximum penetration of PV generation can be increased up to 4.69%, to 10,504.21 kW, when all switches are closed.

By considering Volt/VAr control, Table II shows that the maximum penetration of PV generation can be increased by another 38.79%, to 8,254.36 kW, in relation to the initial radial configuration. By closing branch 12-22, the PV penetration can be increased by a further 23.26%, to 10,174.00 kW. The maximum PV penetration that can be achieved in this case is 10,530.28 kW, which represents an increase of 3.50% in relation to the solution with one loop.

By performing network reconfiguration, without Volt/VAr control (see Table III), the PV penetration can be increased by another 71.92%, to 10,224.64 kW, in relation to the initial radial configuration. Note that this solution presents a hosting capacity for PV generation 0.50% higher than the solution obtained for Case II when one loop is allowed in the network. Moreover, in this case, by allowing closed-loop topologies, the PV penetrations can be increased up to 2.73%, to 10,504.21 kW, when all switches are closed. Moreover, it can be verified that the solutions obtained for Cases I and III with five loops are the same because both cases are equivalent, i.e., without considering Volt/VAr control and with all switches closed.

Finally, by analyzing Table IV, it is possible to verify that the penetration of PV generation can be increased by a further 72.55%, to 10,262.46 kW, in relation to the initial radial configuration. By allowing the formation of more loops in the network, the PV penetration can be increased by more 2.61%, up to 10,530.28 kW.

Therefore, it can be verified that network reconfiguration with simultaneous Volt/VAr control can provide more flexible solutions to the problem. For example, the solution with only one loop obtained in Case IV has a maximum PV hosting capacity that is 0.06% higher than the solution with three loops of Case II. Since the formation of many loops may bring problems to the network operation [19], the proposed approach can provide more suitable solutions to the problem.

The computational times to solve all cases are always lower than four minutes.

2) 85-node network

Tables V–VIII present the results for the 85-node network for Cases I–IV, respectively. These tables provide the total PV hosting capacity of the network, the generation integration at nodes 12/29/58/82, the network topology, represented by the open switches, and information on the expected values of CO_2 emissions. Moreover, only the solutions that present radial configuration, one loop, and the optimal number of loops (that present the highest penetration of PV generation) are presented in these tables.

Results presented in Table V show that the maximum value of PV generation that can be integrated into the 85-node network disregarding any modification in the network is 53,578.06 kW. It can also be verified that the maximum penetration of PV generation can be increased by a further 13.97%, to 61,061.49 kW, by allowing one loop in the network. Note that, except for branch 14-18, which was closed, the states of all other branches in the system remain unchanged in the solution with one loop. Thus, only the value of the PV generation installed at node 12 is increased, since this node is part of the formed loop. The values of PV generation installed at nodes 58 and 82 are the same when comparing the solution with radial topology and the solution with one loop, while the difference in the PV generation installed at node 29 is negligible (around 0.005%). Moreover, by allowing 12 loops in the network, the maximum penetration of PV generation can be increased 7.21%, to 65,461.19 kW.

By analyzing Table VI, it can be observed that the maximum PV hosting capacity of the network considering the original radial topology but performing Volt/VAr control is 53,703.35 kW. It is 0.23% higher than the value for the original topology disregarding Volt/VAr control. On the other hand, by closing one single branch in the network, the PV hosting capacity of the network increases 16.32% to 62,466.25 kW. In addition, a network topology with a single open switch allows increasing the PV hosting capacity of the network to 66,590.01 kW.

Considering Case III, Table VII shows that the radial network reconfiguration allows a PV hosting capacity of 60,789.01 kW which is 13.46% higher than the PV hosting capacity of the original radial topology of the network. This value increases 5.02% when the network reconfiguration considers one loop in the topology. On the other hand, the solution with 8 basic loops in the network allows a PV penetration

TABLE VII
RESULTS FOR THE 85-NODE NETWORK – CASE III: CONSIDERING NETWORK RECONFIGURATION AND NOT CONSIDERING VOLT/VAR CONTROL

Results	Radial	1 Loop	8 Loops
Total PV generation installed (kW)	60,789.01	63,840.76	65,666.78
PV generation installed at nodes 12/29/58/82 (kW)	17,621.31/ 14,563.84/ 17,000.67/ 11,603.19	22,733.78/ 12,002.52/ 17,436.53/ 11,667.92	29,459.77/ 11,759.24/ 14,294.12/ 10,153.65
Open switches	6-7, 33-34, 38-39, 75-76, 5-55, 11-43, 12-72, 14-18, 16-26, 20-83, 28-32, 34-46, 53-64	5-6, 37-38, A-43, 45-46, 53-54, 60-61, 75-76, 12-72, 16-26, 20-83, 28-32, 40-42	27-28, 53-54, 60-61, 20-83, 28-32
Emissions from the main grid (tonnes)	351,732.61	345,594.99	342,237.16
Emissions from the DG (tonnes)	929.60	604.83	686.00
Total emissions (tonnes)	352,662.21	346,199.81	342,923.16

TABLE VIII
RESULTS FOR THE 85-NODE NETWORK – CASE IV: CONSIDERING BOTH NETWORK RECONFIGURATION AND VOLT/VAR CONTROL

Results	Radial	1 Loop	11 Loops
Total PV generation installed (kW)	63,514.23	65,460.81	66,670.80
PV generation installed at nodes 12/29/58/82 (kW)	16,405.93/ 15,393.80/ 19,864.63/ 11,849.87	22,114.82/ 15,087.70/ 18,773.99/ 9,484.29	27,590.83/ 14,699.39/ 13,470.61/ 10,909.97
Open switches	4-5, 31-32, 38-41, A-43, 5-55, 12-72, 13-76, 14-18, 16-26, 20-83, 28-32, 34-46, 53-64	6-7, A-11, 32-33, 38-39, 51-52, 53-54, 71-72, 13-76, 16-26, 20-83, 28-32, 34-46	5-6, 63-64
Emissions from the main grid (tonnes)	345,470.89	342,754.36	339,751.98
Emissions from the DG (tonnes)	713.62	807.34	728.88
Total emissions (tonnes)	346,184.52	343,561.70	340,480.86

of 65,666.78 kW, which is 8.02% higher than the solution obtained through radial reconfiguration.

As presented in Table VIII, when allowing network reconfiguration and Volt/VAr control, the network has higher values of PV penetrations. Considering radial reconfiguration, the PV penetration is 18.55% higher than the PV penetration allowed with the original network. This PV penetration increases 3.06%, to 65,460.81 kW, with a single loop in the network. Finally, a network topology with 11 basic loops in the one that allows hosting 66,670.80 kW of PV generation, which is the highest PV penetration for this network with the presented consideration.

For the topology with all switches closed, it can be verified that the maximum PV penetration for the 85-node network is 66,558.30 kW when Volt/Var control is considered. For this solution, the values for the PV generation installed at nodes 12/29/58/82 are, respectively, 25,382.84 kW, 10,723.15 kW, 10,708.10 kW, and 19,744.21 kW. The values for the emissions from the main grid and DGs are, respectively, 339,738.56 tonnes and 685.84 tonnes. The total emissions are 340,424.40 tonnes. Note that, for this solution, the value for the maximum PV penetration is lower than the value of maximum PV penetration obtained with 11 basic loops shown in Table VIII (66,670.80 kW). For this system, it can be verified that not necessarily an all-closed-switches operation configuration is the topology with the highest hosting capacity.

Moreover, with only a few loops, it is possible to obtain high-quality solutions for the problem. Note that, as the number of loops in the network increases, the additional increase in the host capacity usually decreases. Thus, it would be adequate to operate the network with only a few loops.

For both networks, the obtained solutions were evaluated with a power flow algorithm, in order to verify the operational limits of the network. It was verified that all solutions presented in this work are feasible.

IV. CONCLUSIONS

This paper presented a novel stochastic mixed-integer second-order cone programming model for the problem of short-term planning of active distribution networks for increasing the photovoltaic (PV) generation hosting capacity of the network. The operational actions included Volt/VAr control and network reconfiguration.

Volt/VAr control was considered through the optimal adjustment of capacitors banks, substations' on-load tap changers, and voltage regulators. Besides that, the formulation considered network reconfiguration with both radial and closed-loop operation.

The obtained results showed a higher capacity for PV generation penetration and CO_2 emissions mitigation when Volt/VAr control and reconfiguration with closed-loop topologies were considered. Moreover, it was demonstrated that more flexibility is achieved when both reconfiguration allowing closed-loop operation and Volt/VAr control are considered simultaneously in the problem. Thus, the alternative of performing Volt/VAr control and network reconfiguration allowing closed-loop topologies in active distribution networks can provide more environmentally friendly and efficient operation schemes postponing the necessity of investments for reinforcing the network structure.

Finally, it is important to highlight that solutions with only a few loops present a high increase in the hosting capacity value in relation to the radial configuration. Additional loops present a lower marginal increase to the value of the hosting capacity, or can even reduce the hosting capacity of the network when almost all switches are closed. Future works will include the lifetime of the switches and Volt/VAr control devices in the formulation.

REFERENCES

[1] J. M. Home-Ortiz, L. H. Macedo, R. Vargas, R. Romero, J. R. S. Mantovani, and J. P. S. Catalao, "Increasing the RES hosting capacity in distribution systems through reconfiguration with closed-loop operation and voltage control," in *2021 International Conference on Smart Energy Systems and Technologies (SEST)*, 2021, pp. 1–6.

[2] A. Ferreira *et al.*, "Economic overview of the use and production of photovoltaic solar energy in Brazil," *Renew. Sustain. Energy Rev.*, vol. 81, pp. 181–191, Jan. 2018.

[3] J. M. Home-Ortiz, M. Pourakbari-Kasmaei, M. Lehtonen, and J. R. S. Mantovani, "Optimal location-allocation of storage devices and renewable-based DG in distribution systems," *Electr. Power Syst. Res.*, vol. 172, pp. 11–21, Jul. 2019.

[4] M. U. Hashmi, D. Deka, A. Busic, L. Pereira, and S. Backhaus, "Arbitrage with power factor correction using energy storage," *IEEE Trans. Power Syst.*, vol. 35, no. 4, pp. 2693–2703, Jul. 2020.

[5] R. Mahat, K. Duwadi, F. B. dos Reis, R. Fourney, R. Tonkoski, and T. M. Hansen, "Techno-economic analysis of PV inverter controllers for preventing overvoltage in LV grids," in *2020 International Symposium on Power Electronics, Electrical Drives, Automation and Motion*

(SPEEDAM), 2020, pp. 502–507.
[6] S. F. Santos, D. Z. Fitiwi, M. Shafie-Khah, A. W. Bizuayehu, C. M. P. Cabrita, and J. P. S. Catalão, "New multistage and stochastic mathematical model for maximizing RES hosting capacity—Part I: problem formulation," *IEEE Trans. Sustain. Energy*, vol. 8, no. 1, pp. 304–319, Jan. 2017.
[7] S. F. Santos, D. Z. Fitiwi, M. Shafie-Khah, A. W. Bizuayehu, C. M. P. Cabrita, and J. P. S. Catalão, "New multi-stage and stochastic mathematical model for maximizing RES hosting capacity—Part II: numerical results," *IEEE Trans. Sustain. Energy*, vol. 8, no. 1, pp. 320–330, Jan. 2017.
[8] A. Dubey and S. Santoso, "On estimation and sensitivity analysis of distribution circuit's photovoltaic hosting capacity," *IEEE Trans. Power Syst.*, vol. 32, no. 4, pp. 2779–2789, Jul. 2017.
[9] X. Chen, W. Wu, B. Zhang, and C. Lin, "Data-driven DG capacity assessment method for active distribution networks," *IEEE Trans. Power Syst.*, vol. 32, no. 5, pp. 3946–3957, Sep. 2017.
[10] H. Wang, S. Wang, Q. Zhao, and J. Wang, "Bi-level optimisation dispatch method for photovoltaic hosting capacity enhancement of distribution buses," *IET Gener. Transm. Distrib.*, vol. 13, no. 23, pp. 5413–5422, Dec. 2019.
[11] J. Yuan, Y. Weng, and C.-W. Tan, "Determining maximum hosting capacity for PV systems in distribution grids," *Int. J. Electr. Power Energy Syst.*, vol. 135, p. 107342, Feb. 2022.
[12] M. Rylander, J. Smith, and W. Sunderman, "Streamlined method for determining distribution system hosting capacity," *IEEE Trans. Ind. Appl.*, vol. 52, no. 1, pp. 105–111, Jan. 2016.
[13] F. Capitanescu, L. F. Ochoa, H. Margossian, and N. D. Hatziargyriou, "Assessing the potential of network reconfiguration to improve distributed generation hosting capacity in active distribution systems," *IEEE Trans. Power Syst.*, vol. 30, no. 1, pp. 346–356, Jan. 2015.
[14] R. A. Jacob and J. Zhang, "Distribution network reconfiguration to increase photovoltaic hosting capacity," in *2020 IEEE Power & Energy Society General Meeting (PESGM)*, 2020, pp. 1–5.
[15] S. Jothibasu, A. Dubey, and S. Santoso, "Two-stage distribution circuit design framework for high levels of photovoltaic generation," *IEEE Trans. Power Syst.*, vol. 34, no. 6, pp. 5217–5226, Nov. 2019.
[16] Y.-Y. Fu and H.-D. Chiang, "Toward optimal multiperiod network reconfiguration for increasing the hosting capacity of distribution networks," *IEEE Trans. Power Deliv.*, vol. 33, no. 5, pp. 2294–2304, Oct. 2018.
[17] D. Ritter, J. F. Franco, and R. Romero, "Analysis of the radial operation of distribution systems considering operation with minimal losses," *Int. J. Electr. Power Energy Syst.*, vol. 67, pp. 453–461, May 2015.
[18] T.-H. Chen, W.-T. Huang, J.-C. Gu, G.-C. Pu, Y.-F. Hsu, and T.-Y. Guo, "Feasibility study of upgrading primary feeders from radial and open-loop to normally closed-loop arrangement," *IEEE Trans. Power Syst.*, vol. 19, no. 3, pp. 1308–1316, Aug. 2004.
[19] R. Vargas, L. H. Macedo, J. M. Home-Ortiz, J. R. S. Mantovani, and R. Romero, "Optimal restoration of active distribution systems with voltage control and closed-loop operation," *IEEE Trans. Smart Grid*, vol. 12, no. 3, pp. 2295–2306, May 2021.
[20] M. R. M. Cruz, D. Z. Fitiwi, S. F. Santos, S. J. P. S. Mariano, and J. P. S. Catalão, "Prospects of a meshed electrical distribution system featuring large-scale variable renewable power," *Energies*, vol. 11, no. 12, Dec. 2018.
[21] D. A. Quijano, J. Wang, M. R. Sarker, and A. Padilha-Feltrin, "Stochastic assessment of distributed generation hosting capacity and energy efficiency in active distribution networks," *IET Gener. Transm. Distrib.*, vol. 11, no. 18, pp. 4617–4625, Dec. 2017.
[22] S. Wang, S. Chen, L. Ge, and L. Wu, "Distributed generation hosting capacity evaluation for distribution systems considering the robust optimal operation of OLTC and SVC," *IEEE Trans. Sustain. Energy*, vol. 7, no. 3, pp. 1111–1123, Jul. 2016.
[23] M. S. S. Abad and J. Ma, "Photovoltaic hosting capacity sensitivity to active distribution network management," *IEEE Trans. Power Syst.*, vol. 36, no. 1, pp. 107–117, Jan. 2021.
[24] R. Čađenović and D. Jakus, "Maximization of distribution network hosting capacity through optimal grid reconfiguration and distributed generation capacity allocation/control," *Energies*, vol. 13, no. 20, p. 5315, Oct. 2020.
[25] F. Ding and B. Mather, "On distributed PV hosting capacity estimation, sensitivity study, and improvement," *IEEE Trans. Sustain. Energy*, vol. 8, no. 3, pp. 1010–1020, Jul. 2017.
[26] L. M. Hajagos and B. Danai, "Laboratory measurements and models of modern loads and their effect on voltage stability studies," *IEEE Trans. Power Syst.*, vol. 13, no. 2, pp. 584–592, May 1998.
[27] M. Lavorato, J. F. Franco, M. J. Rider, and R. Romero, "Imposing radiality constraints in distribution system optimization problems," *IEEE Trans. Power Syst.*, vol. 27, no. 1, pp. 172–180, Feb. 2012.
[28] M. E. Baran and F. F. Wu, "Network reconfiguration in distribution systems for loss reduction and load balancing," *IEEE Trans. Power Deliv.*, vol. 4, no. 2, pp. 1401–1407, Apr. 1989.
[29] J.-P. Chiou, C.-F. Chang, and C.-T. Su, "Variable scaling hybrid differential evolution for solving network reconfiguration of distribution systems," *IEEE Trans. Power Syst.*, vol. 20, no. 2, pp. 668–674, May 2005.
[30] S. Pfenninger and I. Staffell, "Renewables.ninja," 2020. [Online]. Available: https://www.renewables.ninja/. [Accessed: 01-Nov-2020].
[31] R. Fourer, D. M. Gay, and B. W. Kernighan, *AMPL: A modeling language for mathematical programming*, 2nd ed. Duxbury, MA, USA: Thomson, 2003.
[32] IBM, "IBM ILOG CPLEX Optimization Studio 20.1.0 documentation," *2021*. [Online]. Available: https://www.ibm.com/support/knowledgecenter/SSSA5P_20.1.0/COS_KC_home.html. [Accessed: 01-Feb-2021].
[33] "LaPSEE power system test cases repository," 2021. [Online]. Available: http://www.feis.unesp.br/#!/lapsee. [Accessed: 01-Oct-2021].

Juan M. Home-Ortiz received the B.S. and M.S. degrees in electrical engineering from the Universidad Tecnológica de Pereira, Colombia, in 2011 and 2014, respectively, and the Ph.D. degree in electrical engineering from the São Paulo State University (UNESP), Ilha Solteira, Brazil, in 2019. Currently, he is carrying out postdoctoral research with UNESP.

During 2020–2021, he was a Postdoctoral Researcher with INESC TEC, Porto, Portugal. His research interests include the development of methods for the optimization, planning, and control, of electrical power systems.

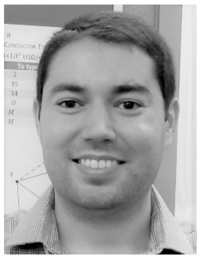

Leonardo H. Macedo (Member, IEEE) received the B.S., M.S., and Ph.D. degrees, all in electrical engineering, from São Paulo State University, Ilha Solteira, Brazil, in 2012, 2015, and 2019, respectively. During 2016–2017, he was a Visiting Student with the University of Washington, Seattle, WA, USA, and from 2019 to 2020, he was a Postdoctoral Researcher with the Universidad de Castilla-La Mancha, Ciudad Real, Spain. He is currently a Postdoctoral Researcher with São Paulo State University.

His current research interests include the development of methods for the optimization, planning, and control of electrical power systems.

Renzo Vargas (Member, IEEE) received the B.S. degree in electrical engineering from the National University Engineering, Lima, Peru, in 2012, and the M.S. and Ph.D. degrees in electrical engineering from São Paulo State University (UNESP), Ilha Solteira, Brazil, in 2015 and 2019, respectively. Currently, he is carrying out postdoctoral research with the Federal University of ABC (UFABC), Santo André, Brazil.

His research interests include the development of methods for the optimization and planning of electrical power systems.

This article has been accepted for publication in a future issue of this journal, but has not been fully edited. Content may change prior to final publication. Citation information: DOI 10.1109/TIA.2022.3177175, IEEE Transactions on Industry Applications

Rubén Romero (Senior Member, IEEE) received the B.S. and P.E. degrees in electrical engineering from the National University of Engineering, Lima, Peru, in 1978 and 1984, respectively. He received the M.S. and Ph.D. degrees in electrical engineering from the University of Campinas, Campinas, Brazil, in 1990 and 1993, respectively. He is currently a full Professor of electrical engineering at São Paulo State University, Ilha Solteira, Brazil.

His research interests include methods for the optimization, planning, and control of electrical power systems, applications of artificial intelligence in power systems, and operations research.

José Roberto Sanches Mantovani (Member, IEEE) received the B.S. degree from São Paulo State University (UNESP), Ilha Solteira, Brazil, in 1981, and the M.S. and Ph.D. degrees from the University of Campinas, Campinas, Brazil, in 1987 and 1995, respectively, all in electrical engineering. He is currently a full professor with the Department of Electrical Engineering, UNESP.

His research interests include the development of methods for the optimization, planning, and control of electrical power systems, and applications of artificial intelligence in power systems.

João P. S. Catalão (Fellow, IEEE) received the M.Sc. degree from the Instituto Superior Técnico (IST), Lisbon, Portugal, in 2003, and the Ph.D. degree and Habilitation for Full Professor (“Agregação”) from the University of Beira Interior (UBI), Covilha, Portugal, in 2007 and 2013, respectively. Currently, he is a Professor at the Faculty of Engineering of the University of Porto (FEUP), Porto, Portugal, and Research Coordinator at INESC TEC. He was the Primary Coordinator of the EU-funded FP7 project SiNGULAR (“Smart and Sustainable Insular Electricity Grids Under Large-Scale Renewable Integration”), a 5.2-million-euro project involving 11 industry partners.

His research interests include power system operations and planning, power system economics and electricity markets, distributed renewable generation, demand response, smart grid, and multi-energy carriers.